Re-evaluation of model-based light-scattering spectroscopy for tissue spectroscopy

Condon Lau
Obrad Šćepanović
Jelena Mirkovic
Sasha McGee
Chung-Chieh Yu
Massachusetts Institute of Technology
George R. Harrison Spectroscopy Laboratory
77 Massachusetts Avenue
Cambridge, Massachusetts 02139

Stephen Fulghum Jr.
Newton Laboratories
23 Cummings Park
Woburn, Massachusetts 01801

Michael Wallace
Mayo Clinic
Department of Gastroenterology and Hepatology
4500 San Pablo Road
Jacksonville, Florida 32224

James Tunnell
University of Texas at Austin
Department of Biomedical Engineering
1 University Station, C0800 Austin
Texas 78712-0238

Kate Bechtel
Michael Feld
Massachusetts Institute of Technology
George R. Harrison Spectroscopy Laboratory
77 Massachusetts Avenue
Cambridge, Massachusetts 02139
E-mail: msfeld@mit.edu

Abstract. Model-based light scattering spectroscopy (LSS) seemed a promising technique for *in-vivo* diagnosis of dysplasia in multiple organs. In the studies, the residual spectrum, the difference between the observed and modeled diffuse reflectance spectra, was attributed to single elastic light scattering from epithelial nuclei, and diagnostic information due to nuclear changes was extracted from it. We show that this picture is incorrect. The actual single scattering signal arising from epithelial nuclei is much smaller than the previously computed residual spectrum, and does not have the wavelength dependence characteristic of Mie scattering. Rather, the residual spectrum largely arises from assuming a uniform hemoglobin distribution. In fact, hemoglobin is packaged in blood vessels, which alters the reflectance. When we include vessel packaging, which accounts for an inhomogeneous hemoglobin distribution, in the diffuse reflectance model, the reflectance is modeled more accurately, greatly reducing the amplitude of the residual spectrum. These findings are verified via numerical estimates based on light propagation and Mie theory, tissue phantom experiments, and analysis of published data measured from Barrett's esophagus. In future studies, vessel packaging should be included in the model of diffuse reflectance and use of model-based LSS should be discontinued. © *2009 Society of Photo-Optical Instrumentation Engineers.* [DOI: 10.1117/1.3116708]

1 Introduction

Improving early detection is the key to managing cancer, since the results of treatment are much more favorable when the cancer is diagnosed at an early, preinvasive stage. To address this, our laboratory has developed trimodal spectroscopy (TMS), a technique that combines three spectroscopic modalities—diffuse reflectance spectroscopy (DRS), intrinsic fluorescence spectroscopy (IFS), and light scattering spectroscopy (LSS). DRS measures the spectrum of diffusely reflected light returning from the tissue and provides information about tissue scattering, blood concentration, and blood oxygenation. IFS measures tissue autofluorescence spectra and provides the relative concentrations of native tissue fluorophores, such as collagen and NADH. In the TMS studies,[1–3] LSS was assumed to measure single elastic light scattering from epithe-

lial nuclei, from which their size distribution could be determined. In this work, we use the term LSS to refer to the specific model-based method employed in those studies, although there are other similarly named methods/techniques that have been developed and used to study single scattering in epithelial nuclei[4–6] and other cell organelles.[7–9]

TMS has shown promise for diagnosing early cancer in a variety of organs, and multipatient, multiorgan studies indicate that LSS was an important predictive component of TMS. Backman et al. applied LSS to detection of early cancer in bladder, colon, and other tissues *in vivo*.[10] They obtained 100% sensitivity and 100% specificity in distinguishing abnormal from normal tissue in bladder and colon. Müller et al. employed TMS in the oral cavity, and obtained 96% sensitivity and 96% specificity in separating cancerous and dysplastic tissues from normal tissue.[3] With LSS alone, they were able to obtain 92% sensitivity and 97% specificity for the same clas-

Address all correspondence to Michael Feld, George R. Harrison Spectroscopy Laboratory, Massachusetts Ave, Cambridge, MA 02139 United States of America; Tel: 617-253-7700; Fax: 617-253-4513; E-mail: msfeld@mit.edu
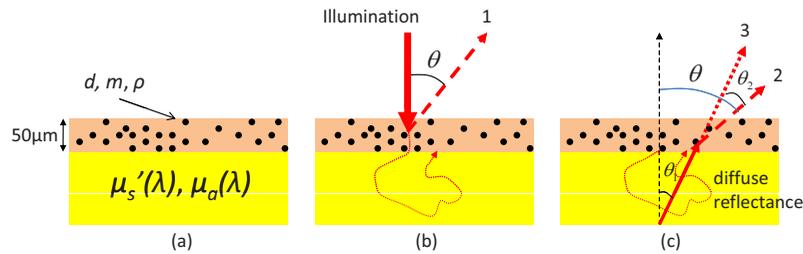
Fig. 1 (a) Two-layer tissue model describing epithelium and subepithelial tissue. d, m, and ρ are the diameter, index mismatch, and number density of spherical scatterers, respectively. $\mu_s{'}(\lambda)$ and $\mu_a(\lambda)$ are the reduced scattering and absorption coefficients of the lower layer, respectively. (b) Backscattering (labeled 1). θ is the angle between the incident beam and a backscattered light ray. The irregularly shaped dotted line represents a light ray entering the diffusive lower layer and re-emerging from the top. (c) Forward scattering (labeled 2) and transmission (labeled 3). θ_1 is the angle between the incident beam and a diffusely reflected light ray exiting the lower layer. θ_2 is the angle of forward scattering. θ is the angle between a forward scattered light ray and the incident beam.

sification. Georgakoudi et al. used TMS in the cervix and were able to distinguish between squamous intraepithelial lesions (SILs) and non-SILs with 92% sensitivity and 90% specificity.[2] With LSS alone, they were able to perform the same distinction with 77% sensitivity and 83% specificity. Georgakoudi et al.[1] employed TMS in Barrett's esophagus and obtained 100% sensitivity and 100% specificity in distinguishing high grade dysplasia from low grade dysplasia and nondysplastic Barrett's. Wallace et al.[11] used LSS alone in Barrett's esophagus and found that dysplasia could be distinguished from nondysplastic tissue with 90% sensitivity and 90% specificity. These studies show that LSS, especially in combination with DRS and IFS, offers promise for diagnosing early cancer.

The LSS modality employed in the previous studies is model based. In model-based LSS, a residual spectrum is obtained by fitting a model of diffuse reflectance to the observed diffuse reflectance spectrum.[12] This residual spectrum was attributed to single elastic light scattering from epithelial nuclei, and a Fourier-transform-based LSS diagnostic algorithm, developed by Perelman et al.[12] and Backman et al.,[10] analyzed it as such to extract nuclear size and density from the wavelength-dependent oscillatory structure.[13] However, recent experimental and theoretical work in our laboratory indicates that this picture is incorrect, and analysis of larger clinical datasets of cervical, oral, and Barrett's esophagus spectra failed to reproduce the results obtained in the original studies[1–3] using model-based LSS. In actuality, the residual spectrum arose primarily from inaccurate modeling of the hemoglobin absorption features in the DRS spectrum. Hemoglobin, a very strong tissue absorber at 420 nm, is contained in blood and confined to the blood vessels. It is thus "packaged" in small regions of the tissue, and this alters the apparent hemoglobin absorption spectrum.[14]

In this work, we provide proof for these claims using numerical estimates based on light propagation and Mie theory, and measurements of reflectance from physiological tissue phantoms. We then analyze the Barrett's esophagus clinical reflectance data of Georgakoudi et al.[1], with and without vessel packaging, to evaluate the role of vessel packaging on DRS fitting. Vessel packaging is a model developed by Svaasand et al. that accounts for the effects of inhomogeneous hemoglobin distribution on diffuse reflectance.[14–16] We conclude by simulating tissue reflectance spectra to show that the Fourier-transform analysis applied to residual spectra is not robust.

2 Elastic Light Scattering Analysis

In this section we employ numerical analysis with light propagation and Mie theory[13] to estimate the magnitude and wavelength dependence of single elastic light scattering from epithelial nuclei relative to the total reflectance. The single scattering contribution is estimated in a background of total reflectance that adds uncertainty to any measurement. A realistic model of light scattering in tissue, first proposed by Perelman et al.,[12] is evaluated, and the amplitudes and spectral shapes of predicted light scattering signals are obtained for later comparison with those acquired in the clinical studies.

Light scattering in epithelial tissue can be modeled by the two-layer tissue model of Fig. 1(a). The lower layer is a semi-infinite diffusive scattering layer with reduced scattering coefficient μ_s' (mm^{-1}) and absorption coefficient μ_a (mm^{-1}), modeling subepithelial tissue. The thin upper layer, representing the epithelium, is composed of spherical scatterers (cell nuclei) of diameter d (μm) and number density ρ (mm^{-3}), with index of refraction mismatch m relative to the surrounding medium. The implementation of Perelman's model presented in this work assumes a single size of epithelial scatterers. This assumption has minimal impact on the final light scattering spectra, because the effect of a distribution of scatterer sizes is similar to the effect of averaging scattering signals measured within a finite solid angle, which is included in the model.

The optical fiber probe used to deliver light and collect tissue spectra in vivo[1–3] consisted of a light delivery fiber surrounded by six collection fibers. All fibers had 200-μm-core diameters and NA=0.22. The fibers were separated from the tissue by a 1.5-mm-thick quartz cover piece. During measurement, the probe was placed in contact with the tissue, and reflectance and fluorescence spectra were acquired. To model this instrument, we make several simplifications to expedite computations. First, the light beam incident on the tissue sample covers the same area as that of the delivery fiber of the probe, but is assumed to be collimated. Second, the fibers are assumed to be in direct contact with the tissue. Therefore,
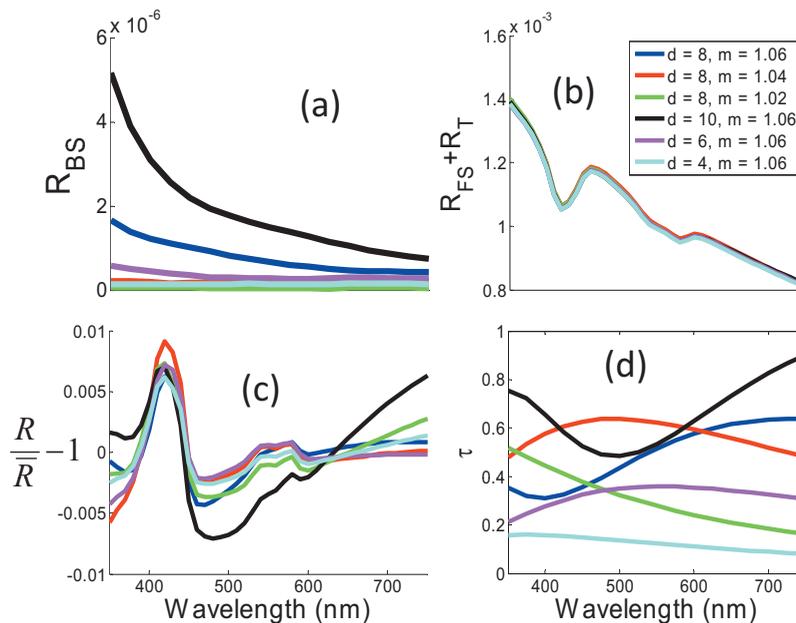
Fig. 2 LSS analysis results computed from histologically relevant epithelial scattering parameters. In the legend, d has units of microns. For all cases $\rho = 8 \times 10^4$ mm^{-3}. (a) Backscattering reflectances. (b) Sum of forward scattering and transmission reflectances. (c) Mean-centered normalized reflectances. (d) LSS features (optical thicknesses) of light scattering from the upper layers.

light returning from the tissue within collection area A (the area on the tissue surface covered by the collection fibers) and collection solid angle Ω_c (the solid angle spanned by NA 0.22 fibers) is collected. To mathematically simulate a tissue reflectance measurement, consider the simplified probe described earlier, placed in contact with the tissue of Fig. 1(a). Light entering the tissue can return to the surface in three ways, as illustrated in Figs. 1(b) and 1(c). 1. The incident light can be backscattered from the upper layer [labeled 1 in Fig. 1(b)]. This light does not enter the lower layer. Light entering the lower layer is diffusely reflected and can return to the surface in two additional ways [dotted and dashed red lines in Fig. 1(c)]. 2. It can be scattered in the forward direction before emerging from the surface [labeled 2 in Fig. 1(c)]. 3. It can traverse the upper layer on the way up without being scattered [labeled 3 in Fig. 1(c)]. The total reflectance (fraction of incident light power collected by the probe) R is the sum of the three contributions:

$$R = R_{BS} + R_{FS} + R_T, \qquad (1)$$

with R_{BS}, R_{FS}, and R_T the reflectance contributions from light collected from area A on the tissue due to backscattering, forward scattering, and transmission, respectively.

Perelman et al. derived expressions for the three reflectance terms, which we express in a form specific to our instrument.

2.1 Backscattering

Consider Fig. 1(b), where θ is the angle between a backscattered light ray and the direction of the incident beam. If we assume R_{BS} to be comprised of only singly backscattered light returning from within the collection area, it can be expressed as follows:

$$R_{BS}(\lambda) = \{1 - \exp[-\tau(\lambda)]\} \int_{\Omega_c} p(\lambda, \pi - \theta) d\Omega. \qquad (2)$$

Here, τ, the optical thickness of the upper layer, is equal to the product of ρ, the layer thickness (assumed to be 50 μm in the simulations), and the total elastic scattering cross section.[13] The wavelength is λ (nm). The single scattering approximation is valid when $T < 1$, a reasonable approximation in the case of tissue epithelium.[17] The factor $1 - \exp[-\tau(\lambda)]$ is the fraction of light scattered once while traversing the upper layer. The phase function of the scatterers in the upper layer $p(\lambda, \pi - \theta)$ can be obtained from Mie theory. The integral over Ω gives the fraction of light scattered into the collection solid angle of the probe.

Figure 2(a) plots R_{BS} for values of d, m, and ρ in the histological range of interest. Note that the backscattering spectrum is smooth, with oscillatory wavelength dependent features having been averaged out by integration over a solid angle.

2.2 Forward Scattering and Transmission

Consider Fig. 1(c). Diffusely reflected light from the lower layer has an approximately Lambertian angular profile. θ_1 is the angle between the incident beam and a light ray emerging from the lower layer. θ is the angle between the incident beam and a diffusely reflected light ray that is forward scattered by the upper layer before reaching the tissue surface. θ_2 is the forward scattering angle. If we assume only transmission or single scattering in the upper layer, and that no light leaks into or out of the collection area during passage through the upper layer, R_{FS} and R_T can be expressed as follows:

$$R_{FS}(\lambda) = \frac{1}{\pi} R_D(\lambda)\{1 - \exp[-\tau(\lambda)]\} \int_{\Omega_c} \int_{2\pi} \cos(\theta_1) p(\lambda, \theta - \theta_1) d\Omega_1 d\Omega, \tag{3}$$

$$R_T(\lambda) = \frac{1}{\pi} R_D(\lambda) \exp[-\tau(\lambda)] \int_{\Omega_c} \cos(\theta_1) d\Omega_1. \tag{4}$$

R_D is the fraction of incident light that traverses the upper layer, is diffusely reflected in the lower layer, and returns to the tissue surface within the probe collection area. The diffuse reflectance model of Zonios et al.,[18] an appropriate extension of the model developed by Farrell, Patterson, and Wilson,[19] provides an analytic solution to R_D in terms of $\mu_s'(\lambda)$, $\mu_a(\lambda)$, and the probe's light delivery and collection areas. The right-hand side of Eq. (3), similar to that of Eq. (2), contains the product of the fraction of light singly scattered and a double integral term representing the fraction of diffusely reflected light scattered into the collection solid angle. Equation (3) requires a double integral with $1/\pi$ and cosine terms, because the angular distribution of diffuse light returning from the lower layer within the collection area is assumed to be Lambertian. Similarly, the right-hand side of Eq. (4) contains the product of the fraction of transmitted light, $\exp[-\tau(\lambda)]$, and an integral representing the fraction of light emitted from the lower layer entering the collection solid angle.

To compute R_D, we model the reduced scattering coefficient as follows:

$$\mu_s'(\lambda) = A\left(\frac{\lambda}{\lambda_0}\right)^{-B} + C\left(\frac{\lambda}{\lambda_0}\right)^{-4}. \tag{5}$$

The reference wavelength $\lambda_0 = 700$ nm. The λ^{-4} term represents a change in the exponent of the reduced scattering coefficient at short wavelengths, which we have observed in modeling data presented in this and other studies. The absorption coefficient used, $\mu_a(\lambda)$, was that of hemoglobin, in which

$$\mu_a(\lambda) = c_{Hb}^*[(1 - \alpha)\varepsilon_{Hb}(\lambda) + \alpha\varepsilon_{HbO_2}(\lambda)], \tag{6}$$

where $c_{Hb}^* = c_{HbO_2} + c_{Hb}$ is the total hemoglobin concentration (mg/mL) in the volume of tissue sampled by light, and $\alpha = c_{HbO_2}/(c_{HbO_2} + c_{Hb})$ is the oxygen saturation. ε_{Hb} is the extinction coefficient of deoxygenated hemoglobin in units of $mm^{-1} \times (mg/mL)^{-1}$, and ε_{HbO_2} is the corresponding extinction coefficient of oxygenated hemoglobin.[20] The reduced scattering and absorption coefficients used in the following elastic light scattering analysis are: $c_{Hb}^* = 1.0$ mg/mL, $\alpha = 0.5$, $A = 1$ mm^{-1}, $B = 0.5$, and $C = 0$ mm^{-1}. A, B, C, α, and c_{Hb}^* are referred to as the spectroscopy parameters. Later in this work, we introduce one additional spectroscopy parameter BVR (effective blood vessel radius), describing vessel packaging. Note that we compute R_D here, assuming a homogeneous hemoglobin distribution rather than a packaged distribution, so we can evaluate the amplitude and spectral shape of epithelial nuclear scattering signals extracted by model-based LSS as implemented in previous works.[1–3,10–12]

Figure 2(b) plots the forward directed reflectance $R_{FS} + R_T$ for values of d, m, and ρ in the histological range of interest. Note that this quantity is two orders of magnitude larger than R_{BS}. Hence, in the total reflectance, the effect of forward directed light dominates over backscattering. Also note that the spectral shape of the forward directed contribution shows features of hemoglobin absorption at 420 and 550 nm. Furthermore, the impact of different upper layers on the total reflectance is small, indicating that the presence of epithelial nuclei has minimal impact on the reflectance measured.

Perelman et al. define the normalized reflectance as:

$$\frac{R}{\bar{R}}, \tag{7}$$

where $\bar{R}$ is the reflectance in the absence of the upper layer. It is not possible to isolate the lower layer during an *in-vivo* measurement, but $\bar{R}$ can be estimated by fitting the diffuse reflectance model of Zonios et al.[18] to R by varying the spectroscopy parameters in Eqs. (5) and (6).[12] For this calculation, we assume that diffusely reflected light exits the tissue with a Lambertian angular profile. The residual spectrum is the wavelength dependent component of $R/\bar{R}$,[12] and this signal was assumed to be due to epithelial nuclear scattering.

We numerically evaluate Eq. (7) for values of d, m, and ρ in the histological range of interest. The results, shown in Fig. 2(c), indicate that the amplitudes, defined as half of the peak-to-peak values of the oscillatory components of the normalized reflectance spectra, are approximately 1% of the total collected light power. Also, the wavelength dependent features of the residual spectra do not have the same frequencies as the LSS features (optical thicknesses) of the upper layers, shown in Fig. 2(d). It is important to note that a one-percent residual spectrum obtained from a clinical experiment would be extremely difficult to detect, given the experimental variability, which is typically 2 to 3 % of the total signal.[2] Further, the fact the residual spectra have different frequencies than the LSS features, contrary to the requirements set by Perelman et al., calls into question the validity of the Fourier-transform analysis.[10,12] The residual spectra of Fig. 2(c) are not in agreement with the LSS features, because the diffusion reflectance model of Zonios et al. used to obtain $\bar{R}$ does not properly account for the addition of a nondiffuse scattering layer on top of a diffuse scattering layer.

3 Tissue Phantom Experiment

In this section we present tissue phantom experiments to verify the findings of the numerical estimates described in the previous section. The phantoms are very similar to the tissue model in Fig. 1(a), with two distinct layers separated by a 100-μm-thick quartz coverslip. The upper layer is 150 μm deep and holds polystyrene spheres (Duke Scientific, Incorporated) of diameter d, in units of microns, immersed in optically clear, refractive index matched oil (Cargille Laboratories) such that m is close to 1. m is varied by using oils of slightly different refractive indexes. The lower layer consists of 10% intralipid (Fresenius Kabi AG) diluted 1:9 with water. This two-layer model is optically similar to tissue, where epithelial nuclei lie on top of a diffuse reflecting stroma.

To create the upper layer, approximately 0.5 mL of the spheres solution was placed inside a vacuum chamber. A
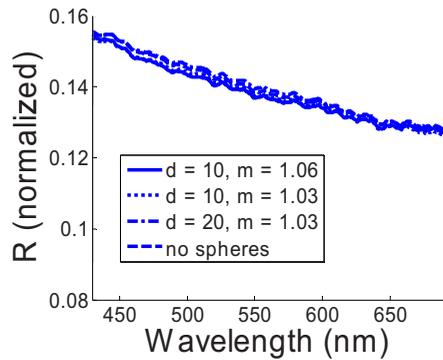
Fig. 3 Reflectance spectra measured from tissue phantoms. The vertical axis is the fraction of light energy collected from the phantom divided by the amount collected from the 99% spectralon. All phantoms had approximately 4×10^4 spheres/mm³ in the upper layer. For clarity, hemoglobin has not been added to the lower layer because the purpose of this phantom is to examine scattering by spheres in the upper layer.

Fig. 4 (a) Reflectance spectrum (solid line) measured from Barrett's esophagus *in vivo* along with optimal fits, using the model of Zonios et al.,[18] with (dotted line) and without (dashed line) vessel packaging to account for the inhomogeneous hemoglobin distribution. We define the optimal fit as the $\bar{R}(\lambda)$ that minimizes $e = \Sigma_\lambda (R(\lambda) - \bar{R}(\lambda)/\bar{R}(\lambda))^2$ over all possible combinations of spectroscopy parameters. For the fit with vessel packaging, $e = 0.35$, and for the fit without vessel packaging, $e = 1.01$. (b) Residual spectra resulting from fitting with (dotted line) and without (dashed line) vessel packaging. The locations of the largest residual features are somewhat arbitrary, as they depend on R and the exact objective function used in the fit optimization. This may affect the appearance of residual spectra presented in other papers, such as in Figs. 3(a) and 3(b) of Perelman et al.[12]

pump was used to evacuate air from the chamber until all of the water had evaporated. Once evaporation was complete, the spheres were removed from the vacuum chamber and approximately 0.5 mL of the index matched oil was placed in the container. The mixture was stirred until the spheres were homogeneously distributed. Lastly, the mixture was placed between two quartz coverslips 150 μm apart to form the upper layer.

We used a probe instrument, very similar to the one used to measure tissue spectra *in vivo*,[1–3] to measure reflectance spectra from four phantoms. The upper layer spheres ranged in diameter from $d = 10$ to 20 μm, and the refractive index mismatch m varied from 1.03 to 1.06. For one phantom, only oil was placed in the upper layer. The measured reflectance spectra, normalized by a measurement of a 99% spectralon standard (Labsphere, Incorporated), are shown in Fig. 3. Even though the upper layer properties vary considerably, the measured reflectance spectra are very similar, as was observed in the previous section [Fig. 2(b)]. This confirms that epithelial nuclear scattering has minimal impact on the total tissue reflectance.

4 Diffuse Reflectance Spectroscopy with and without Vessel Packaging

Previously, residual spectra measured from tissue and similar in form to the ones computed earlier were analyzed with the Fourier-transform analysis[10,12] to extract scatterer size distribution and number density of upper layer structures from the wavelength dependent oscillations.[13] It was assumed that the scatterers were epithelial nuclei with properties in the range listed in Fig. 2(b), and that changes in their properties were related to cancer progression.[12] In this section we analyze a set of reflectance spectra, measured by Georgakoudi et al.,[1] from seven high grade dysplasia (HGD) lesions, seven low-grade dysplasia (LGD) lesions, and 22 nondysplastic Barrett's (NDB) tissue sites. Figure 4(a) shows a representative reflectance spectrum along with its $\bar{R}$ obtained in the same manner as $\bar{R}$ in Eq. (7). The spectroscopy parameters are varied until an optimal fit (defined in the caption of Fig. 4) is obtained.

This is the $\bar{R}$ estimated from the reflectance spectrum assuming a homogeneous hemoglobin distribution in the tissue. In Fig. 4(b), we plot the corresponding normalized reflectance spectrum $(R/\bar{R} - 1)$. The amplitude of the wavelength dependent component of the normalized reflectance spectrum is approximately 10% of the total reflectance. This is an order of magnitude larger than the 1% value computed by elastic light scattering analysis. Therefore, it is unlikely that the origin of the observed residual spectra is due to epithelial nuclear scattering.

Up to this point, we have not discovered the true origin of the 10% residual spectra observed in clinical measurements. To explore this topic, we consider the incorrect assumption made so far in this work that the hemoglobin distribution in tissue is homogeneous. As has been noted by several researchers,[14–16] blood is confined within vessels of finite dimension, thus creating an inhomogeneous distribution of hemoglobin. Because hemoglobin is such a strong absorber at the Soret band (420 nm), regions of tissue with blood vessels can be totally opaque to 420-nm light and be more transparent to other wavelengths. In bulk tissue, this tends to reduce the magnitude of the Soret band relative to the weaker hemoglobin Q bands around 550 nm. Elastic light scattering analysis and corresponding analysis of clinical data suggest that a physical model that more accurately accounts for hemoglobin absorption is required to fit the clinical reflectance spectra. To

address this requirement, we extend DRS to include vessel packaging, which is a model that provides an effective absorption coefficient to account for the effects of an inhomogeneous hemoglobin distribution on diffuse reflectance.

We adopt the vessel packaging derivation of van Veen, Verkruysse, and Sterenborg, and Svaasand et al.,[14,15] and use the correction factor $C_{\text{diff}}(\lambda, BVR)$:

$$C_{\text{diff}}(\lambda, BVR) = \frac{1 - \exp[-2\mu_{a,bl}(\lambda)BVR]}{2\mu_{a,bl}(\lambda)BVR}, \qquad (8)$$

where BVR is the effective blood vessel radius in the tissue volume sampled, and

$$\mu_{a,bl}(\lambda) = 150 \text{ mg/mL} * [(1-\alpha)\varepsilon_{Hb}(\lambda) + \alpha\varepsilon_{HbO_2}(\lambda)] \quad (9)$$

is the absorption coefficient of whole blood. We follow Amelink et al. in using 150 mg/mL as the total hemoglobin concentration in whole blood[21] [this concentration value should not be confused with the average hemoglobin concentration in the volume of tissue sampled, represented by c^*_{Hb} in Eq. (6)]. With this correction factor, one can write the effective absorption coefficient for a volume of tissue containing blood vessels as:

$$\mu_a^{\text{eff}}(\lambda) = C_{\text{diff}}(\lambda, BVR) \times \mu_a(\lambda). \qquad (10)$$

In modeling diffuse reflectance from tissue containing blood vessels, μ_a^{eff} replaces Eq. (6) when computing the fit to a measured diffuse reflectance spectrum with the formula in Ref. 18. During fitting with Eq. (10), we impose a lower limit of 2.5 μm for BVR with the assumption that the minimum blood vessel size should be approximately that of a red blood cell. Compared to fitting done under a homogeneous hemoglobin distribution assumption, an additional spectroscopy parameter, the effective blood vessel radius BVR, is varied.

We define $\bar{R}_{VP}$ as the reflectance measured in the absence of the upper layer for clinical reflectance spectra with vessel packaging included in the model of diffuse reflectance. To estimate $\bar{R}_{VP}$, we fit the reflectance spectra to the model in Ref. 18 by varying the spectroscopy parameters A, B, C, c^*_{Hb}, α, and BVR in Eqs. (6) and (10). With vessel packaging, the fits to the clinical diffuse reflectance spectra improve significantly, and consequently the amplitudes of the residual spectra are greatly reduced. In every case, the fit using vessel packaging is as good or better than the fit without vessel packaging, as is demonstrated for a representative spectrum in Fig. 4(a). The residual spectrum with vessel packaging has smaller amplitude than the residual spectrum without vessel packaging included [Fig. 4(b)]. The ratio of the Soret band dip (~420 nm) to the Q band dips (~540 and 580 nm) in tissue diffuse reflectance spectra is generally smaller than in the homogeneous hemoglobin absorption spectrum. As a result, inclusion of vessel packaging improves the diffuse reflectance fits and accounts for much of the residual spectra previously associated with epithelial nuclear scattering.

5 Numerical Simulations

In this section, we use numerically generated data to show how the effects of the spatially inhomogeneous hemoglobin

distribution on diffuse reflectance could have been misinterpreted as light scattering signals from epithelial nuclei.

Numerical reflectance data with the effects of packaged hemoglobin included were generated as follows. The spectroscopy parameters that define μ_s' in Eq. (5) and μ_a^{eff} in Eq. (10) were chosen to mimic the parameters obtained from the previously published tissue data.[1] The spectroscopy parameters were varied over the following physiological ranges: $0.1 < A < 3$ mm^{-1}, $0.001 < B < 1$, $0 < C < 1$ mm^{-1}, $0 < c^*_{Hb} < 25$ mg/mL, $0 < \alpha < 1$, and $0.0025 < BVR < 0.02$ mm. The resulting combinations of scattering and absorption coefficients were then inputted into the model of Zonios et al. to compute diffuse reflectance spectra. Lastly, random Gaussian noise of varying magnitudes between 50 and 150% of the typical noise magnitude observed during actual clinical measurements was added to each of the spectra. The end result is a series of numerically simulated reflectance spectra spanning all combinations of spectroscopy parameters and noise magnitudes.

The reflectance spectra generated before were then fit to the model by Zonios et al. by varying the spectroscopy parameters in Eqs. (5) and (6) to obtain $\bar{R}$. Note that these fits do not include vessel packaging in the model of diffuse reflectance to be consistent with the previous studies.[1–3,10–12] LSS analysis was then conducted on the residual spectra using the Fourier transform method[12] to extract epithelial nuclei parameters.

Since the numerically generated reflectance data did not include vessel packaging in the model of diffuse reflectance, the fits led to large residual spectra. By applying Fourier-transform analysis on the residual spectra over the wavelength range of 380 to 700 nm, the approximate wavelength range used by Georgakoudi et al.,[1] yielded epithelial nuclei parameters that are consistent with observed nuclear sizes.[22] For example, the mean nuclear diameter extracted varied from 11 to 14 μm, a range readily observed during histopathology. However, the extracted epithelial nuclei parameters were significantly affected by the wavelength range used in the Fourier-transform analysis, the concentration of hemoglobin present in the simulated reflectance spectra, and the magnitude of the noise. For example, when the wavelength range of the analysis was changed from 350 to 700 nm to 390 to 700 nm, the values for the extracted mean diameter and the percentage of enlarged nuclei shifted by 3 μm and 40%, respectively. Figure 5 shows the effects of noise magnitude on the extracted percent nuclear enlargement, a key diagnostic parameter in the original study.[1,3,10,11] The figure shows that extracted values of nuclear enlargement are significantly affected by measurement noise. Since the epithelial nuclei parameters should not vary significantly with experimentally observed levels of noise, the Fourier-transform analysis is not robust. In other words, the performance of model-based LSS in a given dataset depends on fitting strategy.

6 Discussion and Conclusion

In a previous clinical study,[1] the residual spectra had amplitudes an order of magnitude larger than estimates based on light propagation and Mie theory. These mistakenly large val-
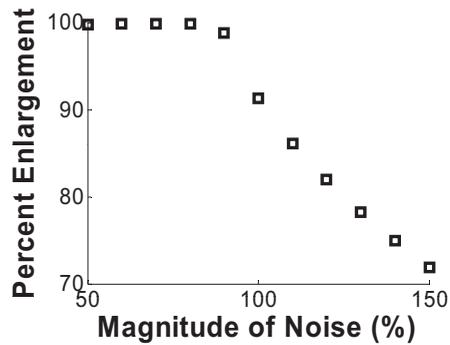
Fig. 5 The effect of varying magnitude of measurement noise on extracted percent nuclear enlargement. Percent enlargement corresponds to the percentage of nuclei with diameters exceeding 10 μm.[10] The average noise magnitude in a clinically measured tissue spectrum corresponds to 100%, but the noise level has been observed to vary from approximately 50 to 150% of the average magnitude.

ues were primarily due to the fact that the original DRS analysis, which used Eq. (6) during fitting, assumed hemoglobin in the tissue to be homogeneously distributed. This gave rise to wavelength dependent features in the residual spectra that were incorrectly attributed to light scattering from epithelial nuclei. In actuality, the distribution of hemoglobin is inhomogeneous. After incorporating vessel packaging to account for the hemoglobin distribution, the amplitudes of the residual spectra are greatly reduced. It is important to note that factors other than neglecting vessel packaging, such as experimental noise and additional absorbers, may also have contributed to the residual spectra. The results presented in this work indicate conclusively that epithelial nuclear scattering is not a significant contributor to the clinically observed diffuse reflectance spectra.

The results of this work and the findings of other researchers[14–16] show that vessel packaging should be included in modeling diffuse reflectance from tissue. Also, analysis of the influence of various parameters (e.g., wavelength range, hemoglobin concentration, noise magnitude) on the extracted epithelial nuclei parameters indicates that the Fourier-transform analysis is not robust. Further, the epithelial nuclear scattering picture is nonphysical. Therefore, in future studies, vessel packaging should be included in the model of diffuse reflectance, and use of model-based LSS should be discontinued. It is important to note that the conclusions presented in this work are restricted to model-based LSS inferred from residual spectra and do not apply to other similarly named methods/techniques that have been developed and used to study single scattering in epithelial nuclei[4–6] and other cell organelles.[7–9]

References

1. I. Georgakoudi, B. C. Jacobson, J. Van Dam, V. Backman, M. B. Wallace, M. G. Muller, Q. Zhang, K. Badizadegan, D. Sun, G. A. Thomas, L. T. Perelman, and M. S. Feld, "Fluorescence, reflectance, and light-scattering spectroscopy for evaluating dysplasia in patients with Barrett's esophagus," *Gastroenterology* **120**(7), 1620–1629 (2001).
2. I. Georgakoudi, E. E. Sheets, M. G. Muller, V. Backman, C. P. Crum, K. Badizadegan, R. R. Dasari, and M. S. Feld, "Trimodal spectroscopy for the detection and characterization of cervical precancers in vivo," *Am. J. Obstet. Gynecol.* **186**(3), 374–382 (2002).
3. M. G. Muller, T. A. Valdez, I. Georgakoudi, V. Backman, C. Fuentes, S. Kabani, N. Laver, Z. Wang, C. W. Boone, R. R. Dasari, S. M. Shapshay, and M. S. Feld, "Spectroscopic detection and evaluation of morphologic and biochemical changes in early human oral carcinoma," *Cancer* **97**(7), 1681–1692 (2003).
4. V. Backman, R. Gurjar, K. Badizadegan, L. Itzkan, R. R. Dasari, L. T. Perelman, and M. S. Feld, "Polarized light scattering spectroscopy for quantitative measurement of epithelial cellular structures in situ," *IEEE J. Sel. Top. Quantum Electron.* **5**(4), 1019–1026 (1999).
5. C. C. Yu, C. Lau, J. W. Tunnell, M. Hunter, M. Kalashnikov, C. Fang-Yen, S. F. Fulghum, K. Badizadegan, R. R. Dasari, and M. S. Feld, "Assessing epithelial cell nuclear morphology by using azimuthal light scattering spectroscopy," *Opt. Lett.* **31**(21), 3119–3121 (2006).
6. A. Wax, C. H. Yang, V. Backman, K. Badizadegan, C. W. Boone, R. R. Dasari, and M. S. Feld, "Cellular organization and substructure measured using angle-resolved low-coherence interferometry," *Biophys. J.* **82**(4), 2256–2264 (2002).
7. M. Hunter, V. Backman, G. Popescu, M. Kalashnikov, C. W. Boone, A. Wax, V. Gopal, K. Badizadegan, G. D. Stoner, and M. S. Feld, "Tissue self-affinity and polarized light scattering in the Born approximation: A new model for precancer detection," *Phys. Rev. Lett.* **97**(13), 138102 (2006).
8. H. Fang, M. Ollero, E. Vitkin, L. M. Kimerer, P. B. Cipolloni, M. M. Zaman, S. D. Freedman, I. J. Bigio, I. Itzkan, E. B. Hanlon, and L. T. Perelman, "Noninvasive sizing of subcellular organelles with light scattering spectroscopy," *IEEE J. Sel. Top. Quantum Electron.* **9**(2), 267–276 (2003).
9. J. R. Mourant, M. Canpolat, C. Brocker, O. Esponda-Ramos, T. M. Johnson, A. Matanock, K. Stetter, and J. P. Freyer, "Light scattering from cells: the contribution of the nucleus and the effects of proliferative status," *J. Biomed. Opt.* **5**(2), 131–137 (2000).
10. V. Backman, M. B. Wallace, L. T. Perelman, J. T. Arendt, R. Gurjar, M. G. Muller, Q. Zhang, G. Zonios, E. Kline, T. McGillican, S. Shapshay, T. Valdez, K. Badizadegan, J. M. Crawford, M. Fitzmaurice, S. Kabani, H. S. Levin, M. Seiler, R. R. Dasari, I. Itzkan, J. Van Dam, and M. S. Feld, "Detection of preinvasive cancer cells," *Nature* **406**(6791), 35–36 (2000).
11. M. B. Wallace, L. T. Perelman, V. Backman, J. M. Crawford, M. Fitzmaurice, M. Seiler, K. Badizadegan, S. J. Shields, I. Itzkan, R. R. Dasari, J. Van Dam, and M. S. Feld, "Endoscopic detection of dysplasia in patients with Barrett's esophagus using light-scattering spectroscopy," *Gastroenterology* **119**(3), 677–682 (2000).
12. L. T. Perelman, V. Backman, M. Wallace, G. Zonios, R. Manoharan, A. Nusrat, S. Shields, M. Seiler, C. Lima, T. Hamano, I. Itzkan, J. Van Dam, J. M. Crawford, and M. S. Feld, "Observation of periodic fine structure in reflectance from biological tissue: a new technique for measuring nuclear size distribution," *Phys. Rev. Lett.* **80**(3), 627–630 (1998).
13. H. C. v. d. Hulst, *Light Scattering by Small Particles*, Dover Publications, New York (1981).
14. R. L. P. van Veen, W. Verkruysse, and H. J. C. M. Sterenborg, "Diffuse-reflectance spectroscopy from 500 to 1060 nm by correction for inhomogeneously distributed absorbers," *Opt. Lett.* **27**(4), 246–248 (2002).
15. L. O. Svaasand, E. J. Fiskerstrand, G. Kopstad, L. T. Norvang, E. K. Svaasand, J. S. Nelson, and M. W. Berns, "Therapeutic response during pulsed laser treatment of port-wine stains: Dependence on vessel diameter and depth in dermis," *Lasers Med. Sci.* **10**(4), 235–243 (1995).
16. J. C. Finlay and T. H. Foster, "Effect of pigment packaging on diffuse reflectance spectroscopy of samples containing red blood cells," *Opt. Lett.* **29**(9), 965–967 (2004).
17. V. Backman, "Reflectance spectroscopy for diagnosis of precancerous

changes in human epithelium," PhD thesis, Massachusetts Institute of Technology, Cambridge, MA (1998).

18. G. Zonios, L. T. Perelman, V. M. Backman, R. Manoharan, M. Fitz-maurice, J. Van Dam, and M. S. Feld, "Diffuse reflectance spectroscopy of human adenomatous colon polyps *in vivo*," *Appl. Opt.* **38**(31), 6628–6637 (1999).

19. T. J. Farrell, M. S. Patterson, and B. Wilson, "A diffusion-theory model of spatially resolved, steady-state diffuse reflectance for the noninvasive determination of tissue optical-properties *in vivo*," *Med. Phys.* **19**(4), 879–888 (1992).

20. S. A. Prahl, "Optical properties of hemoglobin," Oregon Medical Laser Center (1999); http://omlc.ogi.edu/spectra/hemoglobin/index.html.

21. A. Amelink, H. J. C. M. Sterenborg, M. P. L. Bard, and S. A. Burgers, "*In vivo* measurement of the local optical properties of tissue by use of differential path-length spectroscopy," *Opt. Lett.* **29**(10), 1087–1089 (2004).

22. S. L. Robbins and R. S. Cotran, "Pathologic basis of disease," **7**, 1598, (1979).